Cambridge Prisms: Coastal Futures

www.cambridge.org/cft

A comparison between regional sea-level projections and observations

Carolina M. L. Camargo[1], Victor Malagón-Santos[2], Jeemijn Scheen[2], Brendan Oerlemans[2,3] and Aimee B.A. Slangen[2,4]

[1]Department of Physical Oceanography, Woods Hole Oceanographic Institution, Woods Hole, USA; [2]Department Estuarine and Delta Systems, NIOZ Royal Netherlands Institute for Sea Research, Yerseke, The Netherlands; [3]Department of Earth Science, Vrije Universiteit Amsterdam, Amsterdam, The Netherlands and [4]Department of Physical Geography, Utrecht University, Utrecht, The Netherlands

Review

Cite this article: Camargo CML, Malagón-Santos V, Scheen J, Oerlemans B and Slangen ABA (2026). A comparison between regional sea-level projections and observations. *Cambridge Prisms: Coastal Futures*, **4**, e5, 1–10
https://doi.org/10.1017/cft.2026.10023

Received: 30 August 2025
Revised: 08 December 2025
Accepted: 13 January 2026

Keywords:
sea-level change; satellite altimetry; internal variability; sea-level projections; climate change

Corresponding author:
Carolina M.L. Camargo;
Email: carolina.camargo@whoi.edu

C.M.L.C., V.M.S., and J.S. joint first authors.

Abstract

Sea-level projections are highly anticipated outcomes of climate model simulations, relevant for coastal management worldwide. Ideally, any model simulation needs to be validated against observations, but this is impossible for the most recent sets of future climate model simulations, which start near to the present day (2020). Here, we compare satellite observations of regional sea-level change against projections from the Intergovernmental Panel on Climate Change Fifth Assessment Report for total sea-level change and its individual components over their overlapping period, from 2007–2022. We first test and compare three different methods to reduce the internal variability in the observations, which hampers the comparison with models, in particular for shorter time periods. While all three methods reduce the internal variability, we find the low-frequency component analysis (LFCA) removes most of the internal variability. We find that the regional projections are in good agreement with the LFCA-filtered observations, for 96% of ocean area within the 90% confidence interval. For the total sea level and sterodynamic component, the projections both under- and overestimate the observations, depending on the region. For mass-driven sea-level change, the regional projections tend to overestimate the observations. Our analysis gives confidence in sea-level projections for the instrumental era.

Impact statement

Global sea level is rising because of human-induced climate change. Projections of future sea level are published every couple of years in Assessment Reports (ARs) from the Intergovernmental Panel on Climate Change. These projections provide valuable information for coastal management around the world, as measures to adapt to sea-level change need to be planned well in advance. It is therefore important that the projections are reliable, which can be assessed in hindsight by comparing them to observations, when enough time has passed. In this study, we compare the sea-level projections from AR5, which start in 2007, to satellite observations for the period 2007–2022. Whereas previous studies have done similar comparisons for global mean sea level, we perform this comparison for regional sea level. Since the observations have an inherently different (higher) variability and timing than the projections, which particularly complicates comparisons over short time periods, before comparing, we first reduce the variability in the observations with three different methods, inspired by previous research. We identify low-frequency component analysis as the best performing method. We assess the projections of total sea-level change and its separate components: the sterodynamic (thermal expansion, halosteric variations, plus regional changes in oceanic and atmospheric dynamics) and mass (melting land ice) components. We show that the regional projections are in good agreement with the observations, as their 90% confidence intervals overlap in most of the ocean area, giving confidence in sea-level projections for the instrumental era.

Introduction

Present-day sea level is changing as a result of human-induced climate change (Fox-Kemper et al., 2021), impacting low-lying coastal areas around the world. Sea-level change is primarily driven by changes in ocean density and dynamics, by variations in the amount of water stored on land (land ice and land water) and by vertical land motion (for instance, from tectonics, fluid extraction or glacial isostatic adjustment). As a result of these different drivers, sea-level change strongly varies in space and time.

Because of their relevance to coastal communities and decision-makers, projections of future (global and regional) sea-level change are among the most sought-after outcomes of Intergovernmental Panel on Climate Change (IPCC) reports. Building on previous IPCC reports, the

© The Author(s), 2026. Published by Cambridge University Press. This is an Open Access article, distributed under the terms of the Creative Commons Attribution-NonCommercial licence (http://creativecommons.org/licenses/by-nc/4.0), which permits non-commercial re-use, distribution, and reproduction in any medium, provided the original article is properly cited. The written permission of Cambridge University Press or the rights holder(s) must be obtained prior to any commercial use.

IPCC Fifth Assessment (AR5) report was the first IPCC report to assess regional sea-level projections, including the mass change contributions from land ice and land water. These were based on phase 5 of the Coupled Model Intercomparison Project (hereafter CMIP5; Taylor et al., 2012) global climate models for the ocean density and dynamics contribution in combination with dedicated models and parameterizations for ice sheets, glaciers, land water and glacial isostatic adjustment (Church et al., 2013a). This development arose from research into regional sea-level projections using climate models (e.g., Slangen et al., 2012; Perrette et al., 2013) and was followed by intensive research on the topic in the period following AR5 (see, e.g., Garner et al., 2018, for an overview). In particular, the development of probabilistic approaches (e.g., Kopp et al., 2014), the use of physics-based emulators (e.g., Palmer et al., 2020; Yuan and Kopp, 2021) and a strong research community focus on the cryospheric contributions to sea-level change (IMBIE, Otosaka et al., 2023; ISMIP6, Nowicki et al., 2016; and GlacierMIP, Hock et al., 2019) have led to significant advances in sea-level projections since AR5, which could be assessed in the IPCC AR6 report (Fox-Kemper et al., 2021).

Ideally, any model simulation is validated by observations to assess confidence in the results, to improve the models and to enhance process understanding. However, for projections of the future, such a validation is, of course, not possible at the time of publication. What can be done instead is to (i) compare model simulations of the historical period to observations (for sea level, this is done in, e.g., Church et al., 2013c; Meyssignac et al., 2017; Slangen et al., 2017) or to (ii) compare projections that have been made in the past – for instance, IPCC AR5 projections, which are available from 2007 onwards – against observed changes since that time (e.g., Lyu et al., 2021; Wang et al., 2021; Slangen et al., 2023).

The latter comparison is not trivial, because the overlapping time period is relatively short and, in particular, the regional observations contain significant internal variability, with a different regional distribution (both in timing and in magnitude) than the model projections (Figure 1). Using different approaches, projection-observation comparisons have successfully been carried out for global mean sea-level (GMSL) change (Wang et al., 2021; Slangen et al., 2023), for tide gauge locations (Wang et al., 2021) and for the ocean warming component (Lyu et al., 2021). Here, for the first time, we compare the regional sea-level projections (total and contributions) from AR5 to satellite altimetry observations for the period 2007–2022.

To facilitate the comparison to the regional sea-level projections from the CMIP5 climate model ensemble, we present and compare three different methods to reduce the internal variability, which impacts regional observations of sea-level change over shorter time periods: low-frequency component analysis (LFCA), multiple variable linear regression (MVLR) and self-organizing maps (SOMs) (see Methods). We then compare the AR5 model projections to the filtered observations. In addition, we break down regional sea-level change into its two main components: (1) sterodynamic sea level (SDSL), which represents changes due to density and circulation variations, and (2) the mass contribution, where water and ice mass exchanges between land and ocean lead to a gravitational, rotational and viscoelastic deformation response of the solid Earth.

Data

Observations

Absolute sea-level change is obtained from satellite altimetry observations, using the MEaSUREs gridded sea-surface height anomalies product, version 2205 (Fournier et al., 2022). The original data are

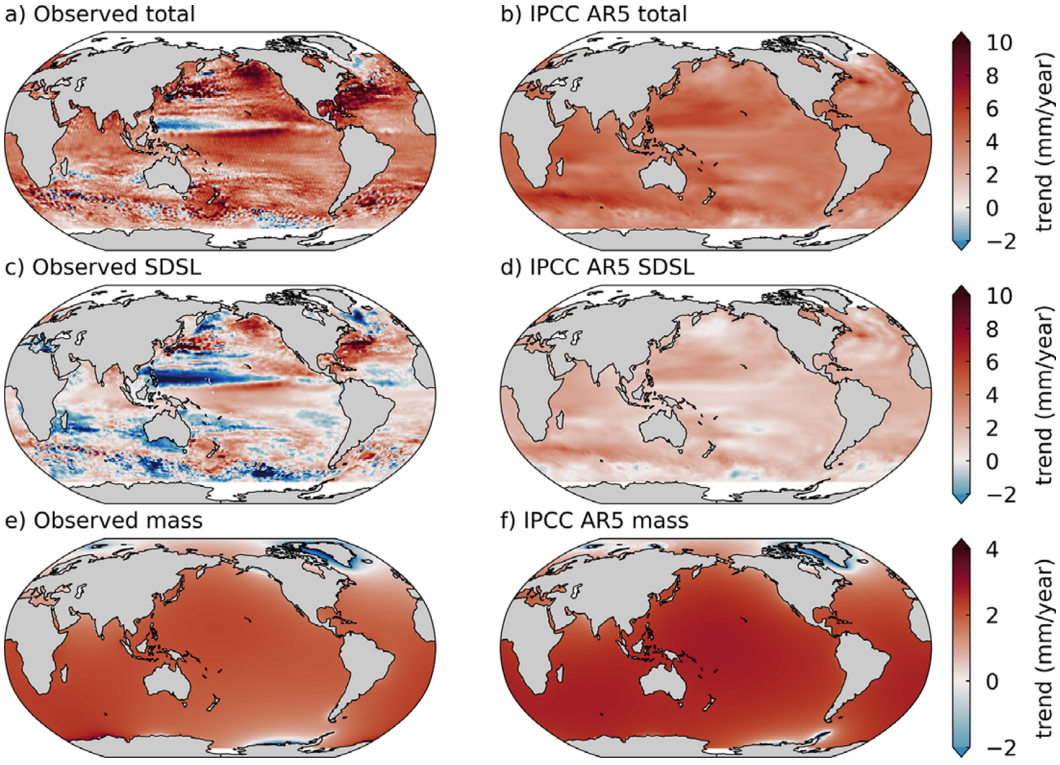


Figure 1. Trends from observed (a) regional sea-level change, (c) sterodynamic sea-level (SDSL) change and (e) mass redistribution, for the period 2007–2022 (see Methods section for observation details). The corresponding IPCC AR5 projections under the RCP4.5 scenario are shown in (b), (d) and (f), respectively.

https://doi.org/10.1017/cft.2026.10023 Published online by Cambridge University Press

provided every 5 days and at a 0.17 × 0.17 degrees resolution. Since the sea-level projections represent relative sea-level change and satellite altimetry represents absolute sea level, we convert the altimetry data by applying corrections for ocean bottom deformation (Frederikse et al., 2017) and glacial isostatic adjustment with the ICE 6G VM5a model (Argus et al., 2014; Peltier et al., 2015). For both corrections, we linearly extrapolate the available data until 2022.

Observed SDSL is based on the ensemble mean of three ocean reanalyzes from the Global Ocean Ensemble Physics Reanalysis product (Copernicus Marine Service Information [CMEMS], 2024). This product provides the output for three different simulations, namely GLORYS2V4, ORAS5 and C-GLORSv7, on monthly intervals and at 0.25 × 0.25 degrees resolution. To obtain the SDSL change, we first remove the time-varying global mean from the sea-surface height of each of the reanalysis products. We then add the global mean steric change of each respective reanalysis, computed from the temperature and salinity data, following Camargo et al. (2020), and compute the average of the three products.

For the observed mass-driven sea-level change, we use relative sea-level fingerprints from Camargo et al. (2022) based on satellite gravimetry from GRACE and GRACE-FO JPL mascons (Watkins et al., 2015; Wiese et al., 2023), updated to 2022. The fingerprints are computed individually for the Antarctic ice sheet, the Greenland ice sheet, glaciers and terrestrial water storage by solving the sea-level equation (Farrell and Clark, 1976).

For the filtering, we use monthly data for all observational products (see Methods section), and the filtered data are then averaged into annual means and regridded to a common 1 × 1 degree resolution using bilinear interpolation, to facilitate comparison with the projections. Both the total and SDSL observational estimates are available from January 1993 until December 2022, whereas the mass-driven component spans the period January 2002 to December 2022. Due to low-quality altimetry measurements in high latitudes, we only consider the ocean area between latitudes 66 degrees north and south.

IPCC AR5 sea-level projections

We use the IPCC AR5 regional relative sea-level projections (Church et al., 2013a), which are based on climate model output from 21 CMIP5 models and use Representative Concentration Pathways (RCPs) scenarios. These sea-level projections include contributions from (dedrifted) ocean thermal expansion and ocean dynamics, inverse barometer effect, glaciers' mass changes, ice sheet surface mass balance and ice dynamics contributions, land water storage changes (from groundwater depletion and reservoir impoundment) and glacial isostatic adjustment. We remove the glacial isostatic adjustment contribution from the projections before comparing the projections to the observations. For this study, we use the ensemble mean, 5th and 95th percentiles of the IPCC AR5 projections under the RCP 4.5 scenario (with a radiative forcing of 4.5 W/m^2 by 2,100), but we note that the choice of scenario is not crucial, as for sea-level change the scenarios do not diverge yet in 2022.

Methods

To reduce the internal variability of the observations (total and SDSL), we test and compare three different methods, namely: (1) LFCA, (2) MVLR and (3) SOM. All methods are applied to monthly observational data from 1993 to 2022, to increase the degrees of freedom. The filtered data are then averaged to annual means.

To obtain trends, we compute ordinary least-squares fits, and the reported uncertainties represent the standard error of the linear regression. We compute the root mean square error (RMSE) between the observations and the AR5 projection and use it as a metric to identify the best filtering method.

Low-frequency component analysis (LFCA)

Pattern filtering techniques based on Empirical Orthogonal Functions (EOFs) have proven to effectively reduce internal climate variability by exploiting spatial covariance information contained in a dataset (e.g., Marcos and Amores, 2014; Wills et al., 2018; Wills et al., 2020; Malagón-Santos et al., 2023). Some of these techniques rely on other realizations to compute an ensemble mean (Wills et al., 2020) or on a pre-industrial control simulation (DelSole et al., 2011; Marcos and Amores, 2014) to separate internal natural variability from the forced response. This makes these methods suitable to be applied to modeling experiments featuring such simulations but not to observations. However, LFCA can reduce internal variability using just one single realization (Schneider and Held, 2001; Wills et al., 2018), making it an ideal candidate to be applied to regional observations. Although not strictly necessary, we removed the seasonal cycle before applying LFCA to the observational dataset, so the EOF analysis can focus on other types of variability. We decomposed the signal into 100 EOFs, selecting this value as a trade-off between degrees of freedom to decompose the signal and computational burden. LFCA sorts the 100 spatial patterns (EOFs) and their corresponding time series by the ratio r_k (Eq. [1]), so that the leading anomaly patterns are those that maximize the ratio of low frequency to total variance:

$$r_k = \frac{\tilde{t}_k^{\,T} \tilde{t}_k}{t_k^T t_k}, \tag{1}$$

where t_k is the time series of the k-th EOF pattern, t_k^T its transpose and $\tilde{t}_k$ denotes t_k after applying a low-pass filter, for which we use a linear Lanczos filter (Duchon, 1979) featuring a 5-year low-pass filter. Using a higher low-pass filter did not lead to significantly different results, indicating that 30 years of observational data is probably not sufficient to accurately characterize modes of variability longer than 5 years. This indicates that there is a possibility of the forced signal leaking into internal variability modes, adding an ambiguity to whether the leading mode truly represents the forced response or realized internal variability.

A forced response with reduced internal climate variability can then be constructed by linearly combining the leading anomaly patterns (Wills et al., 2020; Malagón-Santos et al., 2023). To determine the number of leading anomaly patterns that make up the forced response, we built a set of different forced responses by combining distinct leading EOFs. To confirm which forced response did not contain variability associated with internal climate variability modes (Multivariate El Niño Southern Oscillation Index [MEI], Pacific Decadal Oscillation [PDO], Indian Ocean Dipole [IOD] and Southern Annular Mode [SAM]; see MVLR section), we performed a grid point regression analysis between the filtered results and individual climate indices. We observed that only the forced response made of the first leading anomaly pattern led to nonsignificant regression coefficients, indicating the absence of variability driven by internal climate oscillations. Thus, we use only the first leading EOF, which explains around 15% of the total variance of the data set (after removing the seasonal cycle), to represent the forced response. We compare these LFCA-filtered observations with the AR5 projections.

https://doi.org/10.1017/cft.2026.10023 Published online by Cambridge University Press

Multiple variable linear regression (MVLR)

As a second method to reduce the internal variability in satellite altimetry, we perform a MVLR analysis following Wang et al. (2021). Five climate indices are used as physical indicators ('variables') for modes of internal climate variability: the PDO (Mantua et al., 1997), IOD (Saji et al., 1999), SAM (Marshall, 2003), North Atlantic Oscillation (NAO; Hurrell, 1995), and the MEI (Wolter and Timlin, 1998), which is a combination of multiple indices available for the El Niño Southern Oscillation (ENSO). All climate index time series range from at least 1979 to 2022 and are smoothed and filtered following Zhang and Church (2012) and Wang et al. (2021). We apply the following choice of MVLR to each grid cell:

$$\widehat{\mathrm{SL}} = b_0 + b_1 t + b_{\mathrm{MEI}} \cdot \mathrm{MEI} + b_{\mathrm{PDO}} \cdot \mathrm{PDO} + b_{\mathrm{IOD}} \cdot \mathrm{IOD} + b_{\mathrm{SAM}} \cdot \mathrm{SAM} + b_{\mathrm{NAO}} \cdot \mathrm{NAO} + \epsilon, \quad (2)$$

where $\widehat{\mathrm{SL}}(t,\theta,\phi)$ are the sea-level observations under consideration (either total relative sea level from satellite altimetry or SDSL from reanalyzes) and $b_{\mathrm{CI}}(\theta,\phi)$ is the coefficient for the climate index $\mathrm{CI}(t)$, for which we use the regression coefficient between $\mathrm{CI}(t)$ and $\widehat{\mathrm{SL}}(t,\theta,\phi)$ over their common time period. A least-squares linear fit is used to find the intercept $b_0(\theta,\phi)$ and linear trend $b_1(\theta,\phi)$; $\epsilon(t,\theta,\phi)$ is the residual term. Eq. (2) differs from Wang et al. (2021) in that we use all five climate indices everywhere, and we fit a linear trend instead of a quadratic one, because of our shorter observational record. We then remove the regressed climate indices from the observations using

$$\widehat{SL} - b_{MEI} \cdot MEI - b_{PDO} \cdot PDO - b_{IOD} \cdot IOD - b_{SAM} \cdot SAM - b_{NAO} \cdot NAO = b_0 + b_1 \cdot t + \epsilon. \quad (3)$$

With Eq. (3), we obtain the MVLR-filtered sea level, which represents the sea level observations without the influence of the climate variability. Likely due to a combination of these reasons (short record, all five indices together and a linear fit), we do note that the result of the MVLR filtering is sensitive to the choice of which climate index time series are included, in particular for the PDO. Sensitivity tests excluding the PDO term did not yield better results.

Self-organizing maps (SOM)

SOM is an unsupervised neural network method of feature extraction and classification (Kohonen, 1982; Liu et al., 2006). When applied in the time domain, the method identifies clusters with coherent temporal variability. We use the clusters identified by Camargo et al. (2023), obtained by applying SOM on satellite altimetry sea surface height fields from 1993 until 2019, where the clusters represent regions with similar sea-level variability. Using a slightly different time span does not result in significantly different clusters, as shown in Camargo et al. (2023). The clustering is based on a 3 × 3 neural network applied to the Atlantic Ocean, and a 3 × 3 network applied to the Indo-Pacific Ocean, which yields 18 clusters in total. The separation between basins prevents the strong sea-level variability in the Equatorial Pacific from hindering pattern recognition in the Atlantic Ocean. Further detailed information on the method and parameters used can be found in Camargo et al. (2023). In this study, we compute the spatial average of the total observed sea-level change and the SDSL contribution in each of the 18 clusters to reduce the internal variability from the observations.

Results

The observed regional sea-level trends of total sea-level change clearly differ from the AR5 projections (Figure 1a,b), with a slightly lower global mean (3.74 ± 0.12 mm/yr observed compared to 4 ± 0.02 mm/yr projected) and much stronger spatial variability, compared to the smoother fields of the projections. Likewise, the observed SDSL component shows a larger spatial variability (Figure 1c,d) and has a global average of 0.70 ± 0.10, contrasting with higher and smoother projected trends, with a global average of 1.59 ± 0.02 mm/yr. The projected global mean mass-driven sea-level trends are much higher than the observations (2.29 ± 0.01 mm/yr for projections compared to 1.81 ± 0.11 mm/yr for observations), but the regional patterns are broadly in agreement: negative and positive mass trends are present in similar regions for projections and observations (Figure 1e,f). There are exceptions of some coastal regions in West Canada (only negative in the observations) and Antarctica, where in the observations the mass-driven regional sea-level trends are mainly negative close to the West Antarctic coast, but in the projections this occurs mainly around the Antarctic Peninsula. These differences are probably related to the simplified ice mass loss estimates used in the AR5 projections, which did not feature detailed spatial variability in the fields of mass loss on the ice sheets (Church et al., 2013a). Additionally, groundwater extraction is the only terrestrial water storage component included in the projections, and other components, such as reservoir impoundment or changes in natural water storage, could explain some of the differences between observations and projections. As the regional mass-driven sea-level trends do not show a large spatial variability, we do not apply spatial filtering to this component.

Total and SDSL observations (Figure 1a,c) exhibit high variability due to internal climate variability and mesoscale processes (Carson et al., 2019; Jain et al., 2023). This is, for instance, visible in the Western Equatorial Pacific (with negative trends) and western boundary currents (with positive trends). The observations also show negative trends associated with small to mesoscale eddies in the Antarctic Circumpolar Current, and negative trends south of Greenland related to subpolar gyre oscillations (e.g., Chafik et al., 2019). On the other hand, the IPCC AR5 projections (Figure 1b,d) display smoother spatial patterns in the trends, partly due to the coarse model resolution, which does not allow for an accurate representation of small-scale ocean dynamics (Shevchenko and Berloff, 2022). Furthermore, since the AR5 sea-level projections are a multi-model mean over 21 climate models (Church et al., 2013b), the majority of internal climate variability is averaged out in the ensemble mean (Jain et al., 2023), which can explain part of the difference between the observations and projections: climate model ensembles consist of multiple realizations of the climate state, whereas the observations are only one 'realization'. In addition, the internal variability of model simulations is not in phase with observations (e.g., Carson et al., 2019). These issues can all be addressed by filtering the observational data to improve the comparison to projections.

Removing climate variability from observations

To filter the internal variability from the observations, we tested three different methods (Figure 2): (1) the LFCA method, which identifies the principal components related to the high-frequency (internal variability) and low-frequency variability (forcing); (2) the MVLR method, which identifies and removes the impact of internal

https://doi.org/10.1017/cft.2026.10023 Published online by Cambridge University Press

climate variability using climate indices; and (3) the SOM method, which identifies regions with similar sea-level behavior and averages over these regions (see Methods section for details on the three approaches). LFCA captures the major forced trends and effectively smooths out variability, with only some remnants of strong eddy variability related to the circumpolar and western boundary currents. The MVLR method (Figure 2b) removes Pacific-centered variability (e.g., ENSO), but it is less effective for the NAO and in regions with intense ocean dynamics (e.g., western boundary currents). Like LFCA, the SOM (Figure 2c) also averages out most of the internal variability, except for the area of large trends in the Northwest Atlantic, indicating that these trends are present across a larger area.

The global mean changes of the projections and filtered observations have similar trends (Table 1), and are mostly within the uncertainty envelope of the projections, except for MVLR (Figure 2d). We note that, while the filtering methods reduce the regional discrepancies between projections and observations (as discussed in the next paragraph), they can increase the global mean trend difference by 0.5 mm/yr, with the LFCA total sea-level trend on the lower end with 3.5 ± 0.05 mm/yr, and the MVLR trend on the upper end with 4.1 ± 0.54 mm/yr (Table 1).

To quantify the efficiency of the filtering methods on regional sea-level change, we compute the RMSE between regional observations (unfiltered and filtered) and projections. We then compute how much, on average, the RMSE reduces for the filtered observations compared to the RMSE of the unfiltered observations against projections (Table 1). While all methods reduce the RMSE of the observation with relation to the projection, the LFCA filtering causes a stronger reduction. As already indicated in Figure 2, filtering with SOM and LFCA brings the observations closest to the projections. We also look at the standard deviation (SD) of the time series to see how much of the variability the filtering methods reduce. Like for the RMSE, we see that all methods reduce the SD, with LFCA being the most effective one. For SDSL, we also find that LFCA is the most effective method in reducing the spatial variability (Fig. 1 in the Supplementary Appendix).

Table 1. Area-weighted global mean trends of total sea level from IPCC AR5 projections, satellite altimetry observations and altimetry (alt.) observations after filtering using MVLR, SOM and LFCA, over the period 2007–2022

Method	Global mean trend (mm/yr)	SD (mm)	RMSE w.r.t. AR5 (mm)	RMSE reduction (%)
AR5 projection	4.0 ± 0.02	28	n/a	n/a
Satellite altimetry	3.7 ± 0.12	48	31	n/a
MVLR-filtered alt.	4.1 ± 0.54	45	22	29
SOM-filtered alt.	3.8 ± 0.13	28	15	52
LFCA-filtered alt.	3.5 ± 0.05	20	14	55

Note: Standard deviation (SD) (mm), RMSE with regards to AR5 projection (mm) and reduction of RMSE due to filtering (%). Uncertainties represent the standard error of the linear regression.

Comparing regional AR5 projections to observations

As a result of the ensemble averaging of the projections, the majority of the internal variability in the models is removed (Monselesan et al., 2015; Slangen et al., 2015). When we compare the AR5 projections to the unfiltered observations (Figure 3a), we see large RMSE values, especially in highly dynamic oceanic regions, such as the Indo-Pacific region, the western boundary currents and the Antarctic Circumpolar Current. These high RMSE values in the unfiltered comparison (Figure 3a) are not evidence of model failure, but rather the expected result of comparing a

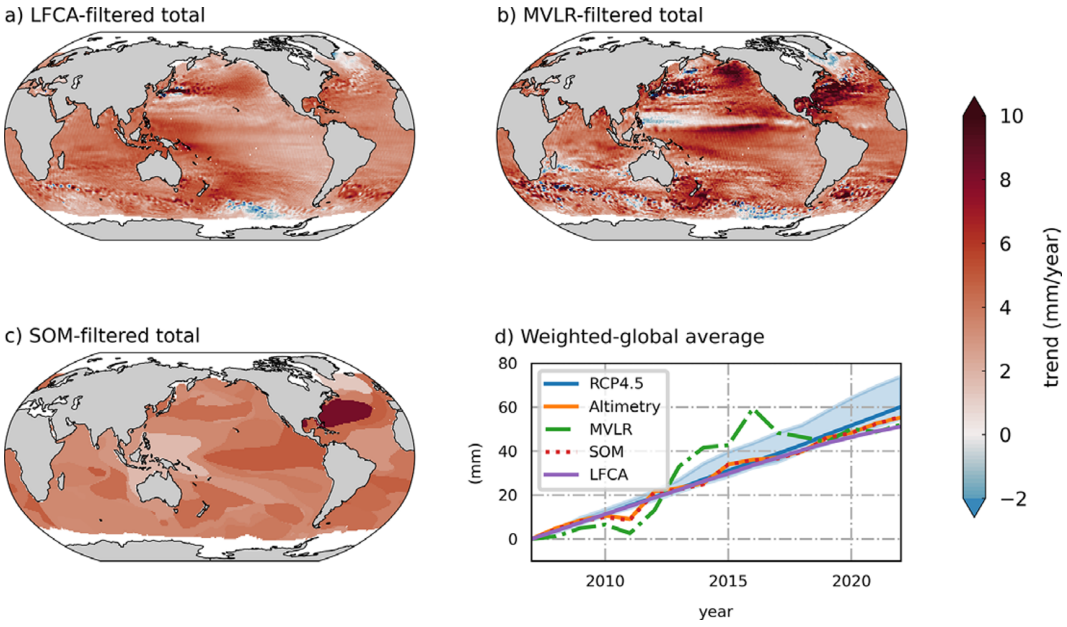


Figure 2. (a–c) Altimetry-observed regional sea-level change trends (mm/yr) for the period 2007–2022 after removing internal variability with (a) low frequency component analysis (LFCA), (b) multiple variable linear regression (MVLR) and (c) self-organizing maps (SOM). (d) Global mean sea-level change with respect to the year 2007, showing the altimetry-observed changes before and after removing variability, and the IPCC AR5 model projections for the RCP4.5 scenario. The shaded area represents the interval between the 5% and 95% percentiles of the ensemble members of the AR5 RCP4.5 scenario projections.

https://doi.org/10.1017/cft.2026.10023 Published online by Cambridge University Press

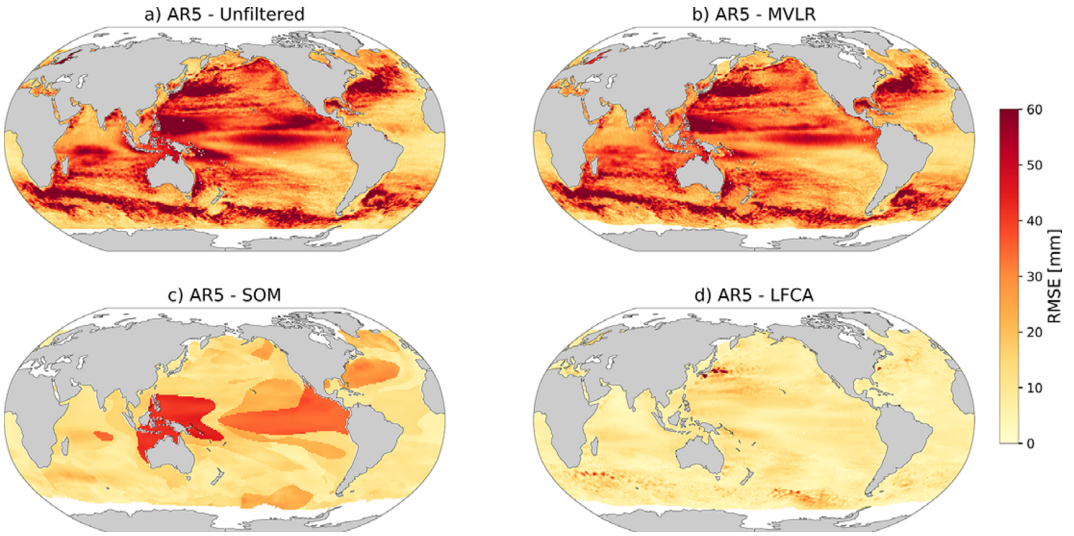


Figure 3. RMSE between IPCC AR5 total sea-level projections and (a) unfiltered, (b) MVLR-filtered, (c) SOM-filtered and (d) LFCA-filtered satellite altimetry observations.

forced-only signal (i.e., the projections) with a dataset containing substantial internal variability (i.e., the unfiltered observations). When we compare the projections with the MVLR-filtered observations (Figure 3b), we see a pattern of RMSE that strongly resembles the RMSE of AR5 versus unfiltered observations. Although the MVLR method should, in principle, remove variability linked to climate modes by incorporating them as predictors, it does not seem effective in this case, possibly because of the limited length of the record. This is in contrast to the SOM and the LFCA methods (Figure 3c and d), which lead to large reductions in the RMSE. The LFCA method is the most successful in isolating the forced response, yielding a small RMSE in most of the regions, with a few exceptions in highly dynamic regions. Thus, we focus on the LFCA method for the remainder of the analysis to highlight the regional agreements and discrepancies between the AR5 and filtered observations. We note, however, that while the LFCA method is the most successful in reducing the RMSE, the LFCA-filtered data might still contain minor remaining internal variability, which cannot be distinguished from the forced signal due to the relatively short time period available for the analysis.

For the total trend (Figure 4b), as well as the SDSL component (Figure 4e), we see that the projections can under- or overestimate the observations depending on the region. For example, most of the equatorial Atlantic is marked by positive anomalies, that is, projections are higher than observations, while in the Eastern Equatorial Pacific, the projections are lower than the observations. The symmetry of the distributions highlights how the projections are both under- and overestimating the observations (Figure 4c,f). The histograms also highlight the efficiency of the different filtering methods in bringing the distribution means closer to zero (i.e., better aligning observations with the projections). The similarities between the anomalies of the total and SDSL components suggest that the differences between the observations and projections are due to sterodynamic processes. The closest agreements between projections and observations are seen for the mass component (Figure 4g–i), with trend anomalies around 0.5 mm/yr, and mainly positive, that is, the mass-driven sea-level projections tend to overestimate the observations. Trend anomalies for the subcomponents of mass-driven sea-level change are presented in Supplementary Appendix Fig. 2.

Discussion

Each filtering method targets the spatiotemporal variability in the observations differently. The LFCA method isolates long-term trends by focusing on low-frequency variability, bringing the observed sea-level trends closer to projections across the Pacific, Indian and Southern Oceans (Figure 3). The MVLR method removes internal climate variability modes like ENSO and NAO, aligning observed trends more closely with projections in areas like the central Pacific, where these oscillations most strongly influence regional sea levels. The SOM method smooths regional variability by clustering areas with similar sea-level trends, helping observations align with projections in broader, less variable regions. However, it retains higher trends in more dynamic regions such as the Northwest Atlantic. Here, we used the method that removed most of the variability across the ocean (LFCA), but if one were interested in a specific area like the Central Pacific and wanted to see what the sea-level trend would be without ENSO, the MVLR method might be better suited to remove the local variability there. The choice of method is therefore dependent on the location and timeframe of interest. Furthermore, the limited record length constrains the robustness of all filtering methods.

In the IPCC AR6 report (Fox-Kemper et al., 2021), the observed global mean sea-level trend was assessed to be 3.69 (3.21–4.17) mm/yr for the period 2006–2018, which is in line with the observed GMSL in Table 1 (which is for a slightly different period). Wang et al. (2021) and Slangen et al. (2023) found that global mean trends of the 2007–2018 observations and AR5 projections were similar, which agrees with our findings for the period 2007–2022. We note that the LFCA filtering does reduce the GMSL trend (by 0.5 mm/yr), suggesting that part of the observed trend could have been increased by internal variability. On a regional scale, however, we see that in some places the (filtered) observations show a larger trend, while in other locations the projections are larger.

Compared with AR5, the more recent IPCC AR6 report (i) presents a slightly lower observed GMSL rate for the period in which they overlap (2006–2018, see Slangen et al. [2023]) and (ii) projects a slightly larger GMSL rise by the end of the twenty-first century, mainly due to a larger projected contribution from the Antarctic ice sheet (see Table 9.8 of Fox-Kemper et al. [2021]). It is, however, too soon to say how the AR6 projections compare against

https://doi.org/10.1017/cft.2026.10023 Published online by Cambridge University Press

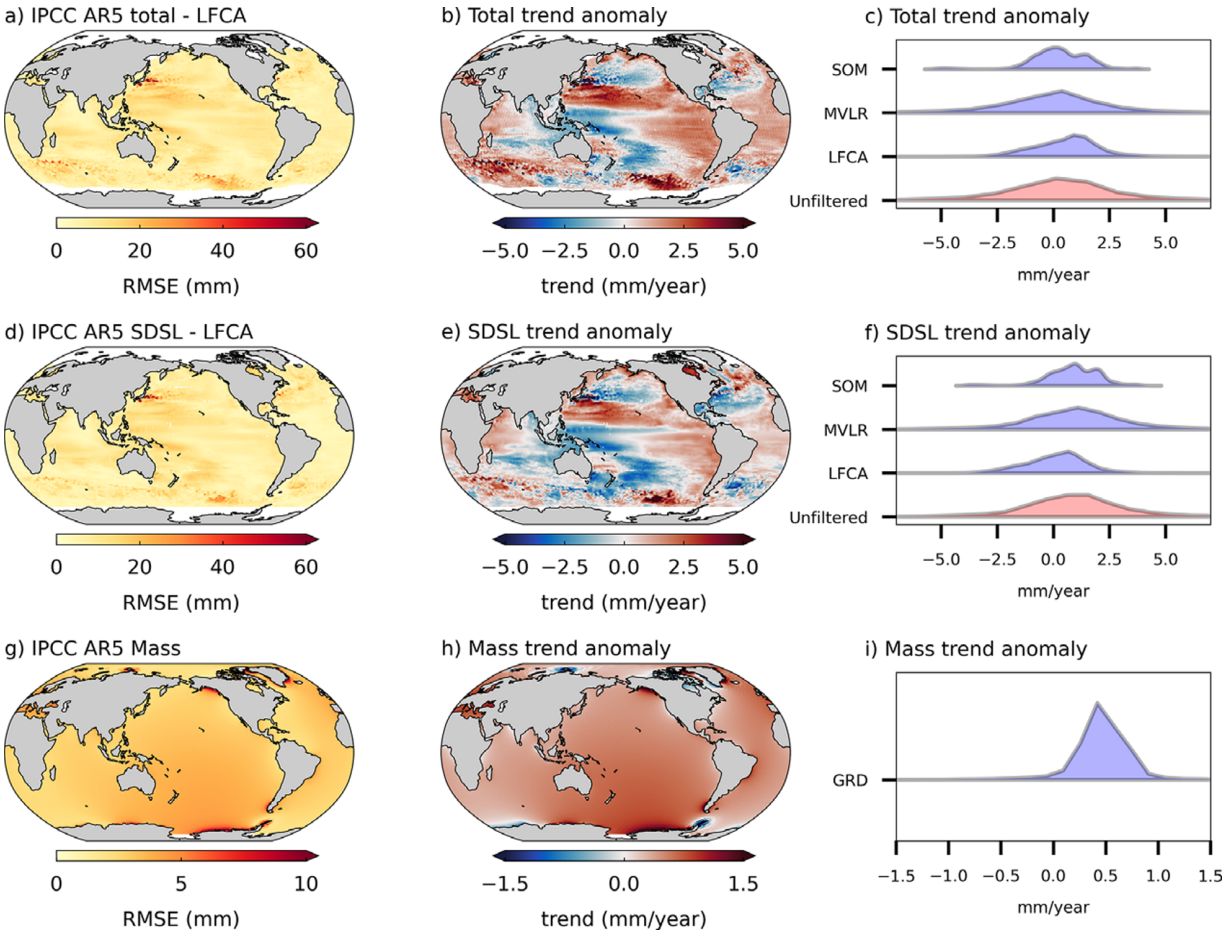


Figure 4. Difference between IPCC AR5 total, SDSL and mass-driven projections (RCP4.5) and (LFCA-filtered) observations, expressed in RMSE (a, d, g), trends anomalies (projections - observations, b, e, h) and trend histograms (c, f, i).

the observations, as the projections are only available from 2020 onwards, so the overlapping period is still too short for a meaningful analysis.

The alignment between filtered observations and projections in the global mean, along with regional matches in many areas, suggests that AR5 projections capture reasonably well externally forced trends. However, some observed regional variability is unaccounted for, particularly in high-dynamic areas. The need for filtering emphasizes that while projections are robust for longer-term, large-scale trends, caution is needed when applying them to regions dominated by large internal climate variability or strong dynamic processes (e.g., boundary currents and eddies), particularly on shorter time scales. The discrepancies between projections and observations, especially the ones related to the SDSL anomalies, could potentially be reduced by using higher spatial resolution models (e.g., Hermans et al., 2020) and by improving the representation of regional ocean dynamics by explicitly modeling mesoscale eddies (Morrison et al., 2016). Regional downscaling could, for instance, better resolve local dynamic effects, and probabilistic approaches could address the variability induced by internal climate oscillations such as ENSO or NAO.

Conclusion

The AR5 projections closely match the observations on a regional scale, especially after filtering is applied to the total sea-level change and the SDSL contribution. For total sea level and SDSL, we find that the AR5 projections both under- and overestimate the observations, depending on the region (see Figure 4b,e). For the mass-driven sea-level component, the projections overestimate the observations almost everywhere, but its impact on the observation-projection discrepancies is smaller than for the SDSL component. The use of filtering methods brings the observed regional trends closer to AR5 projections (reducing the RMSE by $\sim 50\%$), suggesting that a substantial part of the discrepancies arise from internal variability in the observations, whereas this variability is averaged out in the model ensemble, and suggesting that the trends remaining in filtered observations across all methods may be at least partially due to external forcings. Our comparison demonstrates that filtering enhances compatibility between observations and projections, validating the AR5 models for large-scale sea-level trends and highlighting that internal variability affects sea-level observations most in the western boundary currents, Equatorial Pacific and Antarctic circumpolar current. These results provide confidence in using projections for assessing forced sea-level changes, particularly over longer periods and larger regions.

Open peer review. To view the open peer review materials for this article, please visit http://doi.org/10.1017/cft.2026.10023.

Supplementary material. The supplementary material for this article can be found at http://doi.org/10.1017/cft.2026.10023.

Data availability statement. Satellite altimetry can be downloaded at https://podaac.jpl.nasa.gov/dataset/MERGED_TP_J1_OSTM_OST_GMSL_ASCII_V52 (last accessed March/2025), and regional sea level data from IPCC AR5 is

distributed in netCDF format by the Integrated Climate Data Center (ICDC), CEN, University of Hamburg, Hamburg, Germany, at https://www.cen.uni-hamburg.de/en/icdc/data/ocean/ar5-slr.html (last accessed March/2025). Updated steric and mass-driven sea-level change fields, from 2002 to 2022, as well as the altimetry data used, can be found at https://doi.org/10.5281/zenodo.16993112. Filtered altimetry and sterodynamic data can be found at https://doi.org/10.5281/zenodo.16987128. Climate indices were found at NOAA Physical Sciences Laboratory (2023a) for IOD; NOAA Physical Sciences Laboratory (2023b) for MEI; NOAA Physical Sciences Laboratory (2023c) for PDO; NCAR Climate Data (2003) for NAO; and NCAR Climate Data (2023) for SAM. The code to reproduce the analysis can be found at https://github.com/NIOZ-SL/AR5xOBS (https://doi.org/10.5281/zenodo.18620467).

Acknowledgments. Regional sea-level data from IPCC AR5 were distributed in netCDF format by the Integrated Climate Data Center ICDC, CEN, University of Hamburg, Hamburg, Germany. The authors would like to acknowledge the World Climate Research Programme's Working Group on Coupled Modeling, which is responsible for CMIP, and also thank the climate modeling groups for producing and making available their model output.

Author contribution. VMS, CC and JS contributed equally to this manuscript. Conceptualization: CC and AS. Methodology: CC, VMS, JS and AS. Data curation: CC. Data analysis LFCA: VMS. Data analysis MVLR: JS. Data analysis SOM: CC. Data analysis mass-driven estimates: BO. Data visualization: VMS. Supervision: AS. Writing – original draft: CC, JS, VMS and AS. Writing – reviewing and editing: CC, JS, VMS, AS and BO.

Financial support. This publication is part of the project DARSea, awarded to AS (file number VI.Vidi.223.058 of the research program ENW Vidi and Aspasia file number 015.022.013), which is financed by the Dutch Research Council (NWO).

Competing interests. The authors declare none.

References

Argus DF, Peltier WR, Drummond R and Moore AW (2014) The Antarctica component of postglacial rebound model ICE-6G_C (VM5a) based on GPS positioning, exposure age dating of ICE thicknesses, and relative sea level histories. *Geophysical Journal International* **198**, 537–563. https://doi.org/10.1093/gji/ggu140.

Camargo CML, Riva REM, Hermans THJ, Marcos M, Schütt EM, Hernandez-Carrasco I and Slangen ABA (2023) Regionalizing the sea-level BudgetWith machine learning techniques. *Ocean Science* **19**, 17–41. https://doi.org/10.5194/os-19-17-2023.

Camargo CML, Riva REM, Hermans THJ and Slangen ABA (2020) Exploring sources of uncertainty in Steric Sea-level change estimates. *Journal of Geophysical Research: Oceans* **125**, e2020JC016551. https://doi.org/10.1029/2020JC016551.

Camargo CML, Riva REM, Hermans THJ and Slangen ABA (2022) Trends and uncertainties of mass-driven sea-level change in the satellite altimetry era. *Earth System Dynamics* **13**, 1351–1375. https://doi.org/10.5194/esd-13-1351-2022.

Carson M, Lyu K, Richter K, Becker M, Domingues CM, Han W and Zanna L (2019) Climate model uncertainty and trend detection in Regional Sea level projections: A review. *Surveys in Geophysics* **40**, 1631–1653. https://doi.org/10.1007/s10712-019-09559-3.

Chafik L, Nilsen JEØ, Dangendorf S, Reverdin G and Frederikse T (2019) North Atlantic Ocean circulation and decadal sea level change during the altimetry era. *Scientific Reports* **9**, 1041. https://doi.org/10.1038/s41598-018-37603-6.

Church J, Clark P, Cazenave A, Gregory J, Jevrejeva S, Levermann A, Merrifield M, Milne G, Nerem R, Nunn P, Payne A, Pfeffer W, Stammer D and Unnikrishnan A (2013a) Sea level change. In Stocker T, Qin D, Plattner G-K, Tignor M, Allen S, Boschung J, Nauels A, Xia Y, Bex V and Midgley P (eds), *Climate Change 2013: The Physical Science Basis. Contribution of Working Group I to the Fifth Assessment Report of the Intergovernmental Panel on Climate Change*. Cambridge and New York: Cambridge University Press. pp. 1137–1216. https://doi.org/10.1017/CBO9781107415324.026.

Church, JA, Clark PU, Cazenave A, Gregory JM, Jevrejeva S, Levermann A, Merrifield MA, Milne GA , Nerem RS, Nunn PD, Payne AJ, Pfeffer WT, Stammer D and Unnikrishnan AS (2013b) Sea Level Change Supplementary Material. Sea Level Change Supplementary Material. In Stocker T, Qin D, Plattner G-K, Tignor M, Allen S, Boschung J, Nauels A, Xia Y, Bex V and Midgley P (eds), *Climate Change 2013: The Physical Science Basis. Contribution of Working Group I to the Fifth Assessment Report of the Intergovernmental Panel on Climate Change*. Available at www.climatechange2013.org and www.ipcc.ch.

Church JA, Monselesan D, Gregory JM and Marzeion B (2013c) Evaluating the ability of process based models to project sea-level change. *Environmental Research Letters* **8**(1), 014051. https://doi.org/10.1088/1748-9326/8/1/014051.

Copernicus Marine Service Information (CMEMS) (2024) *Global Ocean Ensemble Physics Reanalysis*. Dataset. https://doi.org/10.48670/moi-00024 (accessed 26 August 2024).

DelSole T, Tippett MK and Shukla J (2011) A significant component of unforced multidecadal variability in the recent acceleration of global warming. *Journal of Climate* **24**, 909–926. https://doi.org/10.1175/2010JCLI3659.1.

Duchon CE (1979) Lanczos filtering in one and two dimensions. *Journal of Applied Meteorology and Climatology* **18**, 1016–1022. https://doi.org/10.1175/1520-0450(1979)018<1016:LFIOAT>2.0.CO;2.

Farrell WE and Clark JA (1976) On Postglacial Sea level. *Geophysical Journal of the Royal Astronomical Society* **46**, 647–667. https://doi.org/10.1111/j.1365-246X.1976.tb01252.x.

Fournier S, Willis J, Killett E, Qu Z and Zlotnicki V (2022) *JPL MEaSUREs Gridded Sea Surface Height Anomalies Version 2205* ver 2205. Dataset. https://doi.org/10.5067/SLREF-CDRV3 (accessed 26 August 2024).

Fox-Kemper B, Hewitt H, Xiao C, Aðalgeirsdóttir G, Drijfhout S, Edwards T, Golledge N, Hemer M, Kopp R, Krinner G, Mix A, Notz D, Nowicki S, Nurhati I, Ruiz L, Sallée J-B, Slangen A and Yu Y (2021) Ocean, cryosphere and sea level change. In Masson-Delmotte V, Zhai P, Pirani A, Connors S, Péan C, Berger S, Caud N, Chen Y, Goldfarb L, Gomis M, Huang M, Leitzell K, Lonnoy E, Matthews J, Maycock T, Waterfield T, Yelekçi O, Yu R and Zhou B (eds), *Climate Change 2021: The Physical Science Basis. Contribution of Working Group I to the Sixth Assessment Report of the Intergovernmental Panel on Climate Change*, Chap. 9, Cambridge and New York: Cambridge University Press, pp. 1211–1362. https://doi.org/10.1017/9781009157896.011.

Frederikse T, Riva REM and King MA (2017) Ocean bottom deformation due to present-day mass redistribution and its impact on sea level observations. *Geophysical Research Letters* **44**(24), 12306–12314. https://doi.org/10.1002/2017GL075419.

Garner AJ, Weiss JL, Parris A, Kopp RE, Horton RM, Overpeck JT and Horton BP (2018) Evolution of 21st century sea level rise projections. *Earth's Future* **6**(11), 1603–1615. https://doi.org/10.1029/2018EF000991.

Hermans THJ, Tinker J, Palmer MD, Katsman CA, Vermeersen BLA and Slangen ABA (2020) Improving sea-level projections on the northwestern European shelf using dynamical downscaling. *Climate Dynamics* **54**(3), 1987–2011. https://doi.org/10.1007/s00382-019-05104-5.

Hock R, Bliss A, Marzeion B, Giesen RH, Hirabayashi Y, Huss M, Radić V and Slangen ABA (2019) GlacierMIP – A model intercomparison of global-scale glacier mass-balance models and projections. *Journal of Glaciology* **65**(251), 453–467. https://doi.org/10.1017/jog.2019.22.

Hurrell JW (1995) Decadal trends in the North Atlantic oscillation: Regional temperatures and precipitation. *Science* **269**, 676–679. https://doi.org/10.1126/science.269.5224.676.

Jain S, Scaife AA, Shepherd TG, Zappa G, Smith D, Knight J, Weisheimer A, Schiemann R, Gray L and Ineson S (2023) Importance of internal variability for climate model assessment. *npj Climate and Atmospheric Science* **6**, 68. https://doi.org/10.1038/s41612-023-00389-0.

Kohonen T (1982) Self-organized formation of topologically correct feature maps. *Biological Cybernetics* **43**, 59–69. https://doi.org/10.1007/BF00337288.

Kopp RE, Horton RM, Little CM, Mitrovica JX, Oppenheimer M, Rasmussen DJ, Strauss BH and Tebaldi C (2014) Probabilistic 21st and 22nd century

sea-level projections at a global network of tide-gauge sites. *Earth's Future* **2**(8), 383–406. https://doi.org/10.1002/2014EF000239.

Liu Y, Weisberg RH and Mooers CNK (2006) Performance evaluation of the self-organizing map for feature extraction. *Journal of Geophysical Research: Oceans* **111**(C5). https://doi.org/10.1029/2005JC003117.

Lyu K, Zhang X and Church J (2021) Projected ocean warming constrained by the ocean observational record. *Nature Climate Change* **11**, 834–839. https://doi.org/10.1038/s41558-021-01151-1.

Malagón-Santos V, Slangen ABA, Hermans THJ, Dangendorf S, Marcos M and Maher N (2023) Improving statistical projections of ocean dynamic sea-level change using pattern recognition techniques. *Ocean Science* **19**, 499–515. https://doi.org/10.5194/os-19-499-2023.

Mantua NJ, Hare SR, Zhang Y, Wallace JM and Francis RC (1997) A Pacific interdecadal climate oscillation with impacts on salmon production. *Bulletin of the American Meteorological Society* **78**, 1069–1080. https://doi.org/10.1175/1520-0477(1997)078<1069:APICOW>2.0.CO;2.

Marcos M and Amores Á (2014) Quantifying anthropogenic and natural contributions to thermosteric sea level rise. *Geophysical Research Letters* **41**, 2502–2507. https://doi.org/10.1002/2014GL059766.

Marshall GJ (2003) Trends in the southern annular mode from observations and reanalyses. *Journal of Climate* **16**, 4134–4143. https://doi.org/10.1175/1520-0442(2003)016<4134:TITSAM>2.0.CO;2.

Meyssignac B, Slangen ABA, Melet A, Church JA, Fettweis X, Marzeion B, Agosta C, Ligtenberg SRM, Spada G, Richter K, Palmer MD, Roberts CD and Champollion N (2017) Evaluating model simulations of twentieth-Century Sea-level rise. Part II: Regional Sea-level changes. *Journal of Climate* **30**(21), 8565–8593. https://doi.org/10.1175/JCLI-D-17-0112.1.

Monselesan DP, O'Kane TJ, Risbey JS and Church J (2015) Internal climate memory in observations and models. *Geophysical Research Letters* **42**, 1232–1242. https://doi.org/10.1002/2014GL062765.

Morrison AK, Griffies SM, Winton M, Anderson WG and Sarmiento JL (2016) Mechanisms of Southern Ocean heat uptake and transport in a global eddying climate model. *Journal of Climate* **29**(6), 2059–2075. https://doi.org/10.1175/JCLI-D-15-0579.1.

NCAR Climate Data (2003*) NAO Index Data provided by the Climate Analysis Section (updated regularly) ver Monthly Hurrell North Atlantic Oscillation Index (PC-Based)*. Dataset. Available at https://climatedataguide.ucar.edu/climate-data/hurrell-north-atlantic-oscillation-nao-index-pc-based (accessed 21 June 2023).

NCAR Climate Data (2023) *Marshall Southern Annular Mode (SAM) Index (Station-based)* ver Monthly SAM from Marshall's SAM index page. Dataset. Available at https://climatedataguide.ucar.edu/climate-data/marshall-southern-annular-mode-sam-index-station-based (accessed 21 June 2023).

NOAA Physical Sciences Laboratory (2023a) *Dipole Mode Index (DMI) Monthly Time-series* ver DMI (HadISST). Dataset. Available at https://psl.noaa.gov/data/timeseries/month/DS/DMI/ (accessed 21 June 2023).

NOAA Physical Sciences Laboratory (2023b) *Multivariate ENSO Index Version 2 (MEI.v2)* ver MEI V2 index using the JRA-55 reanalysis dataset. Dataset. Available at https://www.esrl.noaa.gov/psd/enso/mei/ (accessed 21 June 2023).

NOAA Physical Sciences Laboratory (2023c) *Pacific Decadal Oscillation (PDO)* ver ERSST V5. Dataset. Available at https://www.ncei.noaa.gov/access/monitoring/pdo/ (accessed 31 March 2023).

Nowicki SMJ, Payne A, Larour E, Seroussi H, Goelzer H, Lipscomb W, Gregory J, Abe-Ouchi A and Shepherd A (2016) Ice sheet model Intercomparison project (ISMIP6) contribution to CMIP6. *Geoscientific Model Development* **9**(12), 4521–4545. https://doi.org/10.5194/gmd-9-4521-2016.

Otosaka IN, Shepherd A, Ivins ER, Schlegel N-J, Amory C, van den Broeke MR, Horwath M, Joughin I, King MD, Krinner G, Nowicki S, Payne AJ, Rignot E, Scambos T, Simon KM, Smith BE, Sørensen LS, Velicogna I, Whitehouse PL, A G, Agosta C, Ahlstrøm AP, Blazquez A, Colgan W, Engdahl ME, Fettweis X, Forsberg R, Gallée H, Gardner A, Gilbert L, Gourmelen N, Groh A, Gunter BC, Harig C, Helm V, Khan SA, Kittel C, Konrad H, Langen PL, Lecavalier BS, Liang C-C, Loomis BD, McMillan M, Melini D, Mernild SH, Mottram R, Mouginot J, Nilsson J, Noël B, Pattle ME, Peltier WR, Pie N, Roca M, Sasgen I, Save HV, Seo K-W, Scheuchl B, Schrama EJO, Schröder L, Simonsen SB, Slater T, Spada G, Sutterley TC, Vishwakarma BD, van Wessem JM, Wiese D, van der Wal W and Wouters B (2023) Mass balance of the Greenland and Antarctic ice sheets from 1992 to 2020. *Earth System Science Data* **15**(4), 1597–1616. https://doi.org/10.5194/essd-15-1597-2023.

Palmer MD, Gregory JM, Bagge M, Calvert D, Hagedoorn JM, Howard T, Klemann V, Lowe JA, Roberts CD, Slangen ABA and Spada G (2020) Exploring the drivers of global and Local Sea-level change over the 21st century and beyond. *Earth's Future* **8**(9), e2019EF001413. https://doi.org/10.1029/2019EF001413.

Peltier WR, Argus DF and Drummond R (2015) Space geodesy constrains ICE age terminal deglaciation: The global ICE-6G_C (VM5a) model. *Journal of Geophysical Research: Solid Earth* **120**, 450–487. https://doi.org/10.1002/2014JB011176.

Perrette M, Landerer F, Riva R, Frieler K and Meinshausen M (2013) A scaling approach to project regional sea level rise and its uncertainties. *Earth System Dynamics* **4**, 11–29. https://doi.org/10.5194/esd-4-11-2013.

Saji NH, Goswami BN, Vinayachandran PN and Yamagata T (1999) A dipole mode in the tropical Indian Ocean. *Nature* **401**, 360–363. https://doi.org/10.1038/43854.

Schneider T and Held IM (2001) Discriminants of twentieth-century changes in earth surface temperatures. *Journal of Climate* **14**, 249–254. https://doi.org/10.1175/1520-0442(2001)014<0249:LDOTCC>2.0.CO;2.

Shevchenko I and Berloff P (2022) A method for preserving nominally-resolved flow patterns in low-Resolution Ocean simulations: Dynamical system reconstruction. *Ocean Modelling* **170**, 101939. https://doi.org/10.1016/j.ocemod.2021.101939.

Slangen ABA, Church JA, Zhang X and Monselesan DP (2015) The sea level response to external Forcings in historical simulations of CMIP5 climate models. *Journal of Climate* **28**, 8521–8539. https://doi.org/10.1175/JCLI-D-15-0376.1.

Slangen ABA, Katsman CA, van de WRSW, Vermeersen LLA and Riva REM (2012) Towards regional projections of twenty-first century sea-level change based on IPCC SRES scenarios. *Climate Dynamics* **38**(5–6), 1191–1209. https://doi.org/10.1007/s00382-011-1057-6.

Slangen ABA, Meyssignac B, Agosta C, Champollion N, Church JA, Fettweis X, Ligtenberg SRM, Marzeion B, Melet A, Palmer MD, Richter K, Roberts CD and Spada G (2017) Evaluating model simulations of twentieth-Century Sea level rise part I: Global mean sea level change. *Journal of Climate* **30**(21), 8539–8563. https://doi.org/10.1175/JCLI-D-17-0110.1.

Slangen A, Palmer M, Camargo C, Church J, Edwards T, Hermans T, Hewitt H, Garner G, Gregory J, Kopp R, Malagon-Santos V and van de Wal R (2023) The evolution of 21st century sea-level projections from IPCC AR5 to AR6 and beyond. *Cambridge Prisms: Coastal Futures* **1**, e7. https://doi.org/10.1017/cft.2022.8.

Taylor KE, Stouffer RJ and Meehl GA (2012) An overview of CMIP5 and the experiment design. *Bulletin of the American Meteorological Society* **93**(4), 485–498. https://doi.org/10.1175/BAMS-D-11-00094.1.

Wang J, Church JA, Zhang X, Chen X (2021) Reconciling global mean and regional sea level change in projections and observations. *Nature Communications* **12**(1), 990. https://doi.org/10.1038/s41467-021-21265-6.

Watkins MM, Wiese DN, Yuan DN, Boening C and Landerer FW (2015) Improved methods for observing earth's time variable mass distribution with GRACE using spherical cap mascons: Improved gravity observations from GRACE. *Journal of Geophysical Research: Solid Earth* **120**(4). https://doi.org/10.1002/2014JB011547.

Wiese DN, Yuan D-N, Boening C, Landerer FW and Watkins MM (2023) *JPL GRACE and GRACE-FO Mascon Ocean, Ice, and Hydrology Equivalent Water Height CRI Filtered* ver RL06.1Mv03. Dataset. https://doi.org/10.5067/TEMSC-3JC63 (accessed 26 August 2024).

Wills RCJ, Battisti DS, Armour KC, Schneider T and Deser C (2020) Pattern recognition methods to separate forced responses from internal variability in climate model ensembles and observations. *Journal of Climate* **33**, 8693–8719. https://doi.org/10.1175/JCLI-D-19-0855.1.

Wills RC, **Schneider T**, **Wallace JM**, **Battisti DS and Hartmann DL** (2018) Disentangling global warming, multidecadal variability, and El Niño in Pacific temperatures. *Geophysical Research Letters* **45**, 2487–2496. https://doi.org/10.1002/2017GL076327.

Wolter K and Timlin MS (1998) Measuring the strength of ENSO events: How does 1997/98 rank? *Weather* **53**, 315–324. https://doi.org/10.1002/j.1477-8696.1998.tb06408.x.

Yuan J and Kopp RE (2021) Emulating ocean dynamic sea level by two-layer pattern scaling. *Journal of Advances in Modeling Earth Systems* **13**(3), e2020MS002323. https://doi.org/10.1029/2020MS002323.

Zhang X and Church JA (2012) Sea level trends, interannual and decadal variability in the pacific ocean. *Geophysical Research Letters* **39**(21), L21701. https://doi.org/10.1029/2012GL053240.

https://doi.org/10.1017/cft.2026.10023 Published online by Cambridge University Press